

## Ablation of Solids under Femtosecond Laser Pulses

Danny Perez\* and Laurent J. Lewis†

*Département de physique et Groupe de recherche en physique et technologie de couches minces (GCM),  
Université de Montréal, C.P. 6128 Succursale Centre-Ville, Montréal, Québec, Canada H3C 3J7*

(Received 10 May 2002; published 3 December 2002)

We study the basic mechanisms leading to ablation by femtosecond laser pulses using molecular dynamics and a simple two-dimensional Lennard-Jones model. We demonstrate that the ablation process involves three different mechanisms as a function of deposited energy. In particular, it can result from mechanical fragmentation, which does not require the system to cross any metastability or instability line. The relevance of homogeneous nucleation and vaporization for the description of ablation in this regime is also established.

DOI: 10.1103/PhysRevLett.89.255504

PACS numbers: 61.80.Az, 79.20.Ap, 79.20.Ds

The advent of femtosecond lasers in the last 15 years has enabled new insights into the realm of ultrafast dynamics [1,2]. On the femtosecond time scale, energy can be deposited into a material faster than needed for the system to react, leading to confinement of important quantities of energy. This pushes the matter into a state of extreme nonequilibrium (near the critical point, for example) and can lead to material ejection from the target, i.e., ablation.

In spite of numerous efforts [3–8], the fundamental mechanisms that give rise to ultrashort laser ablation have still not been clearly identified. Many different possibilities have been proposed; in particular, homogeneous nucleation of gas bubbles (also known as phase explosion) has frequently been discussed [3,4,7]. This model predicts that the irradiated matter enters the metastable region of the phase diagram (below the binodal line), thereby causing homogeneous nucleation of gas bubbles and eventually dissociation into liquid and gas at high enough nucleation rates. Spinodal decomposition—where the system is brought into the mechanically unstable zone of the phase diagram (below the spinodal line)—has also been invoked [4,5]; in this scenario, ablation results from the phase separation induced by density fluctuations. Finally, complete vaporization of the ejected material has been proposed [6].

These various interpretations suggest that ablation is driven by many different processes. However, experiments also show [4] that different materials behave roughly the same when irradiated by femtosecond pulses at fluences (energy deposited in the target per unit area) below the threshold for plasma formation. This would imply that some very general mechanisms are responsible for the ejection of matter. In this Letter, we study the reaction of a solid to femtosecond laser pulses and the processes that cause ablation using molecular dynamics (MD) and a simple two-dimensional Lennard-Jones model. We show that ablation involves three different processes. One of these is photomechanical fragmentation, identified here for the first time in the context of short-pulses laser ablation: the target disintegrates into

clusters as a result of the mechanical stress imposed by the very rapid thermal expansion of the surface. The other two processes are unambiguously identified as homogeneous nucleation and vaporization. Our study provides the first clear evidence of the relevance of these processes in short-pulse laser ablation conditions.

We chose to study a two-dimensional model as this permits large systems to be explored, thereby minimizing finite-size effects; further, there is no reason to believe that the generic features of laser ablation are different in two and three dimensions. Our system consists of 400 atomic layers in the direction perpendicular to the irradiated surface ( $y$ ) and 500 layers in the lateral direction ( $x$ ), for a total of 200 000 atoms initially forming a triangular lattice. The atoms interact via a Lennard-Jones (LJ) potential with  $\epsilon$  and  $\sigma$  the usual energy and length scales, respectively. In the following, all results are in reduced units, i.e.,  $\epsilon/k_B$  for temperature and  $\tau = (m\sigma^2/\epsilon)^{1/2}$  for time ( $m$  is the atomic mass). The LJ potential was truncated at  $2.5\sigma$ . Before irradiation, the system was fully equilibrated at a low temperature, in the solid phase.

The laser pulse is incident in the  $y$  direction and taken to be spatially constant and Gaussian in time with a width at half maximum of  $0.5\tau$  ( $\sim 100$  fs). The pulse is modeled by a succession of planes, each containing a number of photons determined from the instantaneous irradiance. The energy density deposited by the laser at a given depth follows a Beer-Lambert profile  $e^{-\alpha y}$  with absorption coefficient  $\alpha = 0.01\sigma^{-1}$  [ $\sim (20 \text{ nm})^{-1}$ ]. During absorption, the photon energy is transferred to “carriers.” Here, a carrier is a particle that follows a Drude dynamics with a characteristic scattering time of  $0.005\tau$ . When a collision between a carrier and an atom takes place, a “phonon” of energy  $0.07\epsilon$  ( $\sim 50$  meV) is transferred to the atom if the carrier possesses sufficient energy. This is accomplished by adding an appropriate component (in a random direction) to the velocity of the atom. The carrier cannot absorb energy from the environment. This energy is taken to be  $4.5\epsilon$ , leading to complete relaxation of the gas of carriers within  $0.3\tau$  of the end of the pulse. The

large pressure waves resulting from the rapid heating of the target are absorbed using the boundary conditions described in Ref. [9]. Periodic boundary conditions are used in the  $x$  direction. This model is not meant to reproduce light-matter interactions in a detailed manner; however, it is expected to possess the features which are relevant to a “generic” description of laser ablation at fluences under the threshold for plasma formation.

We first show that ablation proceeds by different mechanisms as a function of the energy density (which varies with depth) imparted to the system and that, in a typical situation, no single process can account for ablation. To demonstrate this, the thermodynamical evolution of the system is followed in time; in this way, it is possible to locate the position (in the phase diagram) at which the creation of defects that eventually leads to ablation is initiated.

In order to obtain the required information, a novel method is introduced, whereby three different thermodynamical trajectories are followed in the  $\rho - T$  phase diagram. The first gives a *macroscopic* (average) view of the system, independent of the presence of clusters or pores. The other two are phase specific: a *dense branch* for atoms belonging to clusters and a *gas branch* for isolated atoms. Clustered atoms are identified using the Hoshen-Kopelman algorithm [10], tuned so that  $\rho_{\text{dense}} > \rho_c$ , where  $\rho_c$  is the density at the critical point. The volume occupied by the different phases is found using the method of Ref. [11]. As we will see, the values of the densities along the different branches give the structural information (porosity and gas content) needed to identify the onset of ablation.

Because the exponential absorption curve gives rise to a nonuniform temperature profile, thermodynamic paths were calculated as a function of depth for groups of atoms having absorbed approximately the same quantity of energy, here four-atomic-layer-thick “slices.” The slices are characterized by an *effective energy density* ( $E_{\text{eff}}$ ), defined as the energy per unit area remaining in the slice after relaxation of the strong thermoelastic pressure built up by the emission of shock waves. Note that the temperatures of the slices were calculated using the velocities relative to the centers of mass. Figure 1 shows the thermodynamic evolution of slices typical of different regions of the target, marked I to IV, each containing many slices, which we discuss next.

The trajectories are of four types. The first, shown in Fig. 1(I), is typical of low absorbed energy densities ( $0 < E_{\text{eff}} < 1.0 \epsilon/\sigma^2$ ). After the constant-volume heating (arrow up) typical of femtosecond laser conditions, the system relaxes within the solid region of the phase diagram. The macroscopic and dense branches coincide, indicating that no voids were created in this slice. As can be verified in the right panel of Fig. 1, no ablation takes place in this region despite the fact that the maximum temperature reached during the simulation is larger

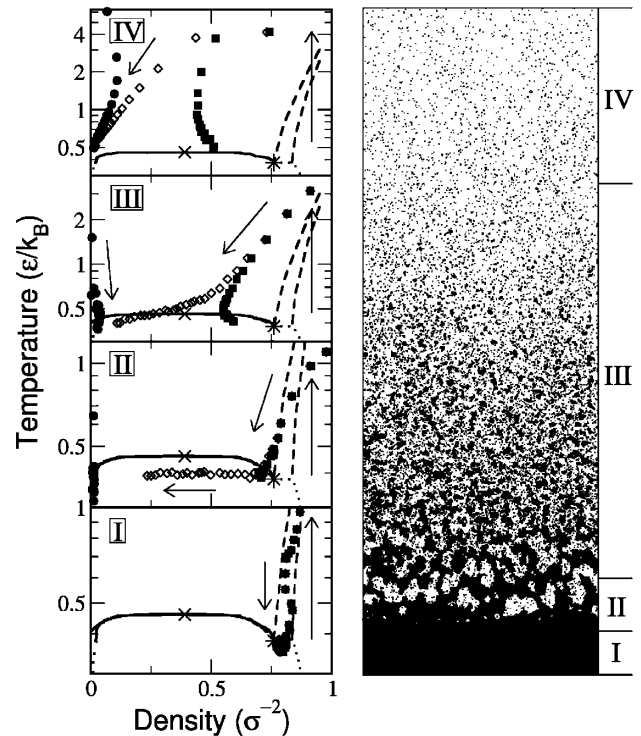


FIG. 1. Left: Time evolution of the system in the  $\rho - T$  plane for different effective energy densities: (I)  $E_{\text{eff}} = 0.7\epsilon/\sigma^2$ , (II)  $E_{\text{eff}} = 1.2\epsilon/\sigma^2$ , (III)  $E_{\text{eff}} = 3.0\epsilon/\sigma^2$ , and (IV)  $E_{\text{eff}} = 6.0\epsilon/\sigma^2$ . Circles: gas branch; squares: dense branch; diamonds: macroscopic branch. Solid line: binodal line [12]; dashed lines: solid-liquid coexistence lines; dotted lines: solid-vapor coexistence lines. The critical point is marked by a cross and the triple point by a star. Arrows indicate the flow of time. Right: Snapshot of a simulation for a fluence of  $F = 900 \epsilon/\sigma$  at  $t = 250\tau$  showing the topology of the system for the four different situations.

than the critical temperature [ $T_c = 0.459 \epsilon/k_B$  [12]] ( $\sim 4000$  K). Relaxation by expansion and conversion of heat into mechanical energy (pressure waves) is thus very efficient in this case.

The medium-energy density situation ( $1.0 < E_{\text{eff}} < 1.3 \epsilon/\sigma^2$ ) is illustrated in Fig. 1(II). The system crosses the solid-liquid coexistence region, then melts when entering the one-phase liquid region. Relaxation continues and the binodal line is crossed. In this case, homogeneous nucleation is expected to occur [13,14], and, indeed, many signs confirm this. First, the creation of pores (marked by the split between the macroscopic and dense branches) occurs only *after* entering the metastable region, the only region in which phase explosion is possible. Second, the gas branch appears at the same moment, indicating that the pores are filled with gas. Third, the phase separation process is evident: the dense phase stays at constant temperature and density inside the metastable region, while the proportion of gaseous atoms steadily increases by nucleation and growth of gas bubbles (see below). This process occurs at nearly constant

temperature because of the following: (i) the free-energy barrier for nucleation of pores is very small for any significant incursion into the metastable region (and vanishes at the spinodal) [15], (ii) only a small fraction ( $\sim 2\%$ ) of the atoms in this slice are actually converted into gas so that the latent heat spent by the system to vaporize these atoms is very small, and (iii) the expansion speed in this region is too small to induce significant cooling. The right panel of Fig. 1 shows that ablation follows as a result of the growth and coalescence of the bubbles.

Our thermodynamical analysis thus *directly* confirms that homogeneous nucleation [3,4] inside the superheated liquid is responsible for ablation in this regime, in contrast with previous MD studies [7], where the occurrence of homogeneous nucleation was inferred from the properties of the ejected material. Because the efficiency of the thermal confinement is typically as strong for picosecond pulses as for femtosecond ones, phase explosion is also expected to occur with longer pulses. However, this kind of trajectory is observed only in a relatively narrow band of absorbed energies, and thus phase explosion cannot solely account for ablation at fluences far above the threshold.

Figure 1(III) shows the typical evolution of the system for energies in the range  $1.3 < E_{\text{eff}} < 4.5 \epsilon/\sigma^2$ . The laser pulse is now intense enough to initially push the sample to a strongly superheated solid state. Thus, melting occurs at the very beginning of the relaxation process. The trajectory differs from that for the phase explosion regime in an important manner: the macroscopic and dense branches now split way *above* the binodal line, *implying that the system has already decomposed by the time the metastable region is reached*. Homogeneous nucleation and spinodal decomposition thus cannot account for ablation in this regime. Given the large number of clusters present in the plume (see right panel of Fig. 1), vaporization must also be excluded. Ablation is therefore *not* caused by a photothermal process [3]. We will return to this crucial point below.

For energies greater than the cohesive energy of the target ( $E_{\text{coh}} = 4.15\epsilon/\sigma^2$ ), complete atomization of the surface layers occurs. This case is presented in Fig. 1(IV). Here, the dense and macroscopic branches split as soon as relaxation starts, and the gaseous and macroscopic branches merge shortly after, indicating that the system behaves essentially like a gas. As can be appreciated from the right panel of Fig. 1, a very small number of atoms form clusters in this region of the plume (so the behavior of the dense branch is not meaningful). This regime thus corresponds to a vaporization process.

As a final note, we have not observed a single case where the critical point was approached while the system was homogeneous; i.e., we find no evidence for spinodal decomposition as reported in Ref. [5].

We have shown that, depending on the energy, three different mechanisms may cause ablation in the femto-second regime. At sufficiently high fluences, all of them are effective in different regions of the target. While two of these processes—homogeneous nucleation and vaporization—are photothermal, the third is not. We now proceed to show that in this third regime, ablation is “photomechanical” and occurs by a fragmentation process.

In the energy density range where ablation is not photothermal, the relaxation of the very large thermoelastic stress induced by the constant-volume heating of the target causes the expansion to proceed at very high speed, itself a strongly varying function of injected energy (and hence of position inside the target). This causes spatially nonuniform strain rates ( $\eta = dv_{\text{translation}}/dy$ ) that can reach values as large as  $\eta = 0.1\tau^{-1}$  ( $10^{12} \text{ s}^{-1}$ ). Under such conditions, the elastic energy stored in the expanding liquid grows very rapidly. Further, the large expansion speed *gradient* will inhibit the diffusion mechanism by which density inhomogeneities (induced by thermal fluctuations) are usually balanced out. These inhomogeneities will thus survive and actually grow, leading the creation of internal surfaces and enabling the relaxation of some internal stresses. If enough surface is created, the initially homogeneous fluid will turn into an ensemble of clusters, and ablation follows. This strain-induced structural reorganization is called fragmentation. It does not require any change of phase, nor the crossing of a metastability or instability limit, and thus can occur in supercritical conditions where phase explosion and spinodal decomposition are not possible. It differs from other photomechanical mechanisms (cavitation [16] or spallation [7]) because it does not involve the passage of tensile waves through the target. In fact, tensile waves do not form in our samples at high fluences.

Ashurst and Holian [17] have observed fragmentation in two- and three-dimensional LJ systems under homogeneous expansion. It has also been observed in studies of the rapid heating of liquid drops [18,19] and in experiments on the free-jet expansion of liquids [20,21]. We now demonstrate quantitatively that fragmentation is indeed responsible for ablation in the high-energy regime.

For fragmentation, the size of the clusters formed should decrease with increasing local strain rate, as larger strain rates cause more surfaces to be created and thus smaller fragments. This is verified in Fig. 2 where the mean cluster mass (at the time they formed) is plotted against the local strain rate for  $F = 750\epsilon/\sigma$ , and is also apparent in region III of the right panel in Fig. 1. In fact, there appears to be a power-law dependence between the two quantities. This dependence can be quantitatively accounted for by the simple fragmentation model of Ashurst and Holian [17], which states that fragmentation results from the conversion of the internal stress stored in the expanding target into surface energy: for a uniaxial

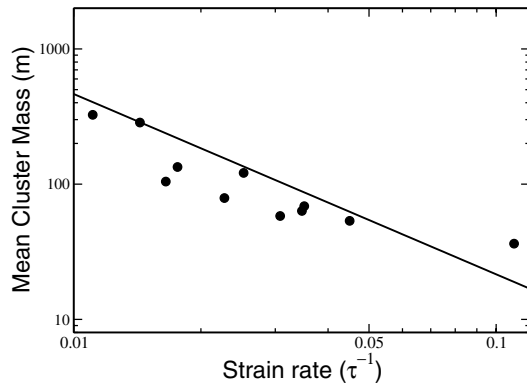


FIG. 2. Mean cluster mass versus local strain rate for  $F = 750\epsilon/\sigma$ . The solid line is Eq. (1) with  $\rho = 0.55\sigma^{-2}$ ,  $\gamma = 0.4\epsilon/m$ , and  $\zeta = \pi/4$  (circular fragments).

expansion in two dimensions, the mean cluster mass depends on the local strain rate as

$$M = 4\zeta\rho(r_0\gamma)^{2/3}\eta^{-4/3}, \quad (1)$$

where  $\zeta$  is a geometric factor of the order of unity,  $\eta$  is the strain rate,  $r_0$  is the equilibrium bond length, and  $\gamma$  is the surface energy per unit mass. The same power-law dependence is predicted by the energy-minimization model of Grady [17,22] and thus constitutes a strong signature of fragmentation. These models are also known to be correct in three dimensions, with a different scaling of the cluster mass on the strain rate.

Equation (1) is plotted in Fig. 2, using  $\rho = 0.55\sigma^{-2}$  as a typical density at fragmentation time,  $\gamma = 0.4\epsilon/m$  and  $\zeta = \pi/4$  (circular fragments). The model accounts precisely for the power-law dependence and the prefactor agrees with the MD data to within 30%. Given the difficulty in evaluating the different parameters entering Eq. (1) in such rapidly changing conditions, the agreement is excellent. Because the fragmented state is not the equilibrium configuration at low densities and high temperatures typical of the diluted plume, many monomers are emitted from the surface of the clusters (see right panel of Fig. 1) in order to restore the equilibrium gaseous state. The Ashurst-Holian prediction is thus valid only at early times. Taken together with the evidence from the thermodynamical trajectories, this shows that fragmentation is indeed responsible for ablation in the nonphoto-thermal regime.

As a final note, for the thermoelastic stress to be released violently enough that important strain rates are induced in the target, the stress confinement condition ( $\tau_p \alpha c < 1$  where  $\tau_p$  is the pulse length and  $c$  is the speed of sound) must be respected. Since this is usually true for picosecond pulses, fragmentation should also occur in this case. Preliminary simulations of our model system in the picosecond regime confirm this.

Our simulations therefore establish that laser ablation in the short-pulse regime involves both thermal and me-

chanical processes, which are effective at different deposited energies' densities (and hence different depths under the surface of the target). Mechanical fragmentation is identified here for the first time in the context of short-pulse laser ablation. The relevance of homogeneous nucleation and vaporization in the description of ablation in this regime is also established.

We thank Patrick Lorazo, Ralf Meyer, and Michel Meunier for numerous enlightening discussions. This work has been supported by grants from the Canadian *Natural Sciences and Engineering Research Council* (NSERC) and Québec's *Fonds québécois de la recherche sur la nature et les technologies* (NATEQ). We are indebted to the *Réseau québécois de calcul de haute performance* (RQCHP) for generous allocations of computer resources.

\*Electronic address: danny.perez@umontreal.ca

†Electronic address: Laurent.Lewis@UMontreal.CA

- [1] A. Rousse *et al.*, *Nature* (London) **410**, 65 (2001).
- [2] A. Cavalleri *et al.*, *Phys. Rev. Lett.* **87**, 237401 (2001).
- [3] R. Kelly and A. Miotello, *Appl. Surf. Sci.* **96-98**, 205 (1996).
- [4] K. Sokolowski-Tinten *et al.*, *Phys. Rev. Lett.* **81**, 224 (1998).
- [5] F. Vidal *et al.*, *Phys. Rev. Lett.* **86**, 2573 (2001).
- [6] B. N. Chichkov *et al.*, *Appl. Phys. A* **63**, 109 (1996).
- [7] L. V. Zhigilei and B. J. Garrison, *J. Appl. Phys.* **88**, 1281 (2000).
- [8] R. Herrmann, J. Gerlach, and E. Campbell, *Appl. Phys. A* **66**, 35 (1998).
- [9] L. V. Zhigilei and B. J. Garrison, *Mater. Res. Soc. Symp. Proc.* **538**, 491 (1999).
- [10] J. Hoshen and R. Kopelman, *Phys. Rev. B* **14**, 3438 (1976).
- [11] A. Strachan, T. Çağın, and W. A. Goddard III, *Phys. Rev. B* **63**, 060103 (2001).
- [12] B. Smit and D. Frenkel, *J. Chem. Phys.* **94**, 5663 (1991).
- [13] N. Inogamov, S. Anisimov, and B. Retfeld, *J. Exp. Theor. Phys.* **88**, 1143 (1999).
- [14] V. Zhakhovskii, K. Nishihara, S. Anisimov, and N. Inogamov, *JETP Lett.* **71**, 167 (2000).
- [15] V. K. Shen and P. G. Debenedetti, *J. Chem. Phys.* **114**, 4149 (2001).
- [16] A. Oraevsky, S. Jacques, and F. Tittel, *J. Appl. Phys.* **78**, 1281 (1995).
- [17] W. T. Ashurst and B. L. Holian, *Phys. Rev. E* **59**, 6742 (1999).
- [18] J. A. Blink and W. G. Hoover, *Phys. Rev. A* **32**, 1027 (1985).
- [19] A. Strachan and C. Dorso, *Phys. Rev. C* **59**, 285 (1999).
- [20] E. L. Knuth and U. Henne, *J. Chem. Phys.* **110**, 2664 (1999).
- [21] W. T. Ashurst and B. L. Holian, *J. Chem. Phys.* **111**, 2842 (1999).
- [22] D. E. Grady, *J. Appl. Phys.* **53**, 322 (1982).